Accepted version of the paper.

Published Version DOI: 10.1007/s10546-016-0149-6

Quantitative interpretation of air radon progeny fluctuations in terms of stability conditions in the atmospheric boundary layer

Roberto Salzano · Antonello Pasini · Giampietro Casasanta · Marco Cacciani · Cinzia Perrino

Received: DD Month YEAR/ Accepted: DD Month YEAR

Abstract Determining the mixing height using a tracer can improve the information obtained using traditional techniques. Here we provide an improved box model based on radon progeny measurements, which considers the vertical entrainment of residual layers and the variability in the soil radon exhalation rate. The potential issues in using progeny instead of radon have been solved from both a theoretical and experimental perspective; furthermore, the instrumental efficiency and the counting scheme have been included in the model. The applicability range of the box model has been defined by comparing radon-derived estimates with sodar and lidar data. Three intervals have been analyzed ("near-stable", "transition" and "turbulent"), and different processes have been characterized. We describe a preliminary application case performed in Rome, Italy, while case studies will be required to determine the range limits that can be applied in any circumstances.

Keywords Aerosols and particles, Boundary-layer processes, Geochemical cycles, Model verification and validation, Modelling.

1 Introduction

The presence of air pollutants in the lower troposphere is highly influenced by meteorological

---

R. Salzano
Institute of Atmospheric Pollution Research, National Research Council of Italy, 50019 Florence, Italy
email: salzano@iia.cnr.it

A. Pasini • C. Perrino
Institute of Atmospheric Pollution Research, National Research Council of Italy, 00015 Rome, Italy

G. Casasanta
Institute of Atmospheric Sciences and Climate, National Research Council of Italy, 00155 Rome, Italy

M. Cacciani
Department of Physics, Sapienza – University of Rome, 00145 Rome, Italy

conditions, which regulate turbulent mixing and the vertical and horizontal components of dispersion. Substances emitted into the atmospheric boundary layer (ABL) are gradually dispersed and eventually become completely mixed within this layer, given sufficient time and if there are no significant sinks (Seibert et al. 2000). The usual definition of the ABL involves considering the ABL to be the turbulent domain of the atmosphere adjacent to the ground. In this case, the ABL coincides with the mixing layer, i.e., a term commonly used in air pollution meteorology. The height of the mixing layer, the so-called "mixing height", determines the available volume for the dispersion of pollutants, and this height is involved in many predictive and diagnostic methods and/or models used to assess pollutant concentrations. Furthermore, this variable is a critical parameter in atmospheric flow models (Lin 2012).

Traditionally, "profile-based" methods have been used to estimate the mixing height; these include direct measurement techniques obtained from remote sensing systems (radar, sodar or lidar) and sensors deployed on platforms (radiosondes, tethered balloons or masts) or aircraft. Furthermore, dynamical models provide fields relevant to the ABL, but the reliability of their performance needs to be better assessed; see, for instance, Nath and Patil (2006).

The scientific community considers the use of ^{222}Rn (radon) to be a comparatively simple and economical approach for defining the stability conditions of the lower troposphere (Duenas et al. 1996, Perrino et al. 2001, Pasini et al. 2003, Sesana et al. 2003, Desideri et al. 2006, Zhang et al. 2006, Desideri et al. 2007, Perrino et al. 2008, Chambers et al. 2011, 2015) and for estimating the mixing height (Pasini and Ameli 2003, Sesana et al. 2003, 2006, Veleva et al. 2010, Keller et al. 2011, Griffith et al. 2013). Earlier Guedalia et al. (1980) described this noble gas as a perfect tracer of ABL dilution features, and demonstrated that radon radioactivity represents a simple index of the stability state of the ABL. Once emitted by soil, radon leaves the surface by molecular diffusion or by convection, and enters the atmosphere where it is distributed by turbulent mixing (Porstendorfer 1994). The radon decay products are metallic elements that are easily fixed to existing aerosol particles in the atmosphere. The reduction of these particles in the atmosphere occurs either by radioactive decay or by removal processes (dry deposition, rainout, washout). The distribution of this aerosol component in the troposphere is controlled mainly by turbulent mixing.

Radioactivity measurements show a typical time variability reaching a maximum concentration during the night, in conditions of strong stability, and a minimum during the day when the mixed layer is well developed and vertical dilution occurs. Otherwise, low quasi-constant values are found in advective situations characterized by mixing due to turbulence. From a qualitative point of view, the activity of ^{222}Rn, or its progeny counts, is proportional to the stability conditions of the lower troposphere. If advection occurs, the contribution of different air masses must be carefully assessed.

A better description of mixing and exchange processes in the ABL under different conditions can be obtained by estimating the vertical radon profile. The vigour of atmospheric mixing, in fact, regulates the vertical radon profile in the ABL (Williams et al. 2011). The structure of the lower troposphere can be simplified with a one-dimensional ABL model, composed of a mixing layer and a residual layer. While the mixing layer is characterized by vertical profiles controlled by meteorological conditions, the residual layer can be described by constant concentrations of radon and its progeny with altitude. The transition between the two layers is usually manifest by a sharp gradient at the top of the mixing layer (Lopez et al. 1974, Vinod Kumar et al. 1999). Therefore, if we assume a homogeneous exchange coefficient in the vertical profile within the stable layer, the approximation of the nocturnal stable layer via a box model is supported (Guedalia et al. 1980). The top of this box, defined as the "equivalent mixing height" (h_e), is a semi-quantitative index of the dispersion properties of this layer; low values of h_e are related to low dispersion power and high concentrations of primary pollutants.

In Guedalia et al. (1980), the calculation of the top of the box was performed by means of

$$h_e = \frac{\phi \Delta t}{C_{[t]} - C_{[0]}}, \qquad (1)$$

where ϕ is the radon flux at the surface, Δt is the time interval from the start of accumulation, $C_{[t]}$ is the radon concentration at time t (Bq m^{-3}) and $C_{[0]}$ is the radon concentration at the beginning of accumulation (Bq m^{-3}). Allegrini et al. (1994) showed that h_e can be properly identified as the height at which a parcel of air emanating from the ground ceases to rise, at least in nocturnal situations where advection is negligible. Furthermore, they quantified the layer depth over a town by coupling a temperature profile from radiosonde ascents made in the suburbs and the near-surface air temperature measured at the radon detection site within the town. The high correlation between the estimated urban mixing height (h_u) and h_e supports the correct estimation of the urban mixing height by the box model, at least when turbulence in the mixing layer is thermally driven. This approach has been tested only under stable and non-advective conditions, with no rain, constant relative humidity, constant atmospheric pressure and a limited space-time interval. This framework implies, first of all, that radon exhalation from the ground is constant over time and spatially homogeneous. If our measurements are progeny-based the box model requires also that: i) the fraction of radon daughters attached to the particulate matter is constant, ii) the equilibrium factor between decay product is constant, iii) the vertical profile is constant through the mixing layer (in the case of single-height observations), and iv) the radon concentration is directly proportional to the number of detected α or β counts. This last issue represents substantially an instrumental component that requires a calibration obtained using a reference material or independent techniques.

Radon can be measured either as an α or β particle emitter associated with the decay of its short-lived progeny. Several instrumental approaches support the determination of the radon concentration in air. Considering continuous techniques only, Frank et al. (2012) classified the available devices used in "one-filter" and "two-filters" systems. The first method is based on measuring the α or β activity directly on the filter through which air is passed. These systems can be equipped with "selective" detectors, capable of discriminating different nuclides at specific energies, or by "gross" detectors, which estimate the total activity emitted by collected particles. The second group is based on a two-step collection that isolates the progeny associated directly with ^{222}Rn present in air. This latter approach represents the reference method in the framework of the Global Atmospheric Watch Programme of the World Meteorological Organization. The operational conditions can be perfectly controlled and the ^{222}Rn measurements in the air are more reliable and sensitive compared to the first group. These systems are more complex than "one-filter" devices and they require more resources in terms of maintenance and logistics. The cost-effectiveness of "one-filter" systems is an important feature that favours the diffusion of this type instead of "research" instruments. These simplified systems introduce, unfortunately, interference due to the contemporary presence of several radon daughters, with different half-lives, and to the variability of disequilibrium between those nuclides and radon in the atmosphere.

From this perspective, the model must include a conversion coefficient that can support the estimation of single-height radon activity based of total β counts, which is affected both by disequilibrium effects and by instrumental efficiency. The aim of the present study is to investigate the use of mixing-height modelling by using radon progeny instead of direct ^{222}Rn measurements. The approach is, firstly, based on a general modification of the box model considering not only nocturnal stable conditions and a variable radon soil exhalation. Secondly, we present a calibration protocol for use in converting progeny observations into radon air activity. Finally, we check the validity of our progeny-based model with ground-based techniques (sodar and lidar).

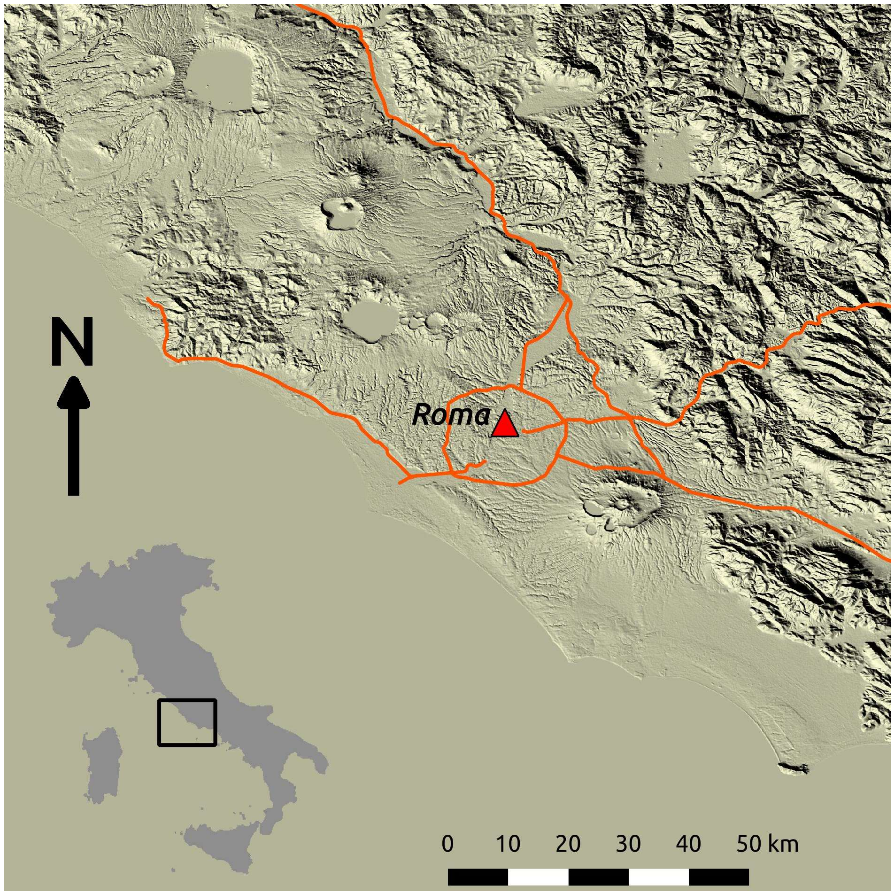

Fig 1 Location map of the study area (Rome, Italy). Red lines represent the major roadways.

2 Methods

The adaptation of a simplified ABL box model to radon-progeny observations required the development of appropriate equations designed to support the comparison between radon-progeny derived mixing height and independent estimates obtained by traditional techniques such as sodar and lidar. Firstly, we present in this section the experimental set-up useful for validating our model. Then we describe from a general point of view our box model and we define the adaptation required to the specific site and instrumentation included in this study case.

2.1 Experimental

We describe the experimental set-up at first, because constraints to the modelling are induced by the study site and by the radon-progeny instrument.

2.1.1 The study site

The field survey was conducted in the city of Rome, Italy, at the Sapienza University Campus (latitude 41°54’05”N, longitude 12°30’57”E). The sampling site (Fig. 1) was on the roof of the Physics Department, approximately 75 m above the sea level, 20 m above the ground. The rooftop facility features standard meteorological sensors that provide air temperature and relative humidity. The observing period commenced on 20 June and concluded on 12 July 2011.

2.1.2 Radon progeny detector

The natural radioactivity was measured using an automatic stability monitor (A PBL Mixing Monitor, FAI Instruments, Fontenuova, Rome, Italy), comprising a sampler for the collection of particulate matter on filter membranes and a Geiger-Muller counter for determining the total β-activity of the short-lived radon progeny attached to the particles. The instrument operates on two filters at the same time: while the sampling phase is acting on one filter for 1 h, the β detection is performed on the other filter. These instrumental features ensure that the short-lived β activity of the particles is continuously determined over an integration time of 1 h and that the β measurement period is long enough to guarantee highly accurate results. The residual radioactivity is taken into account using a software procedure. The accuracy of the determination is improved by the automatic subtraction of the background radiation (Perrino et al. 2000), while the lower limit of detection of the stability monitor has been estimated at 0.15 Bq m^{-3}. This value is affected by the conversion factor (c_f) defined in Section 3.2 (c_f = 0.77 s^{-1} Bq^{-1}) but reference materials are necessary for a more detailed definition of the lower limit of detection. The maximum instrumental error at the lowest counting level was about 3%.

2.1.3 Sodar

The instrument considered in the present study was a fully automated monostatic triaxial Doppler sodar, which allows a continuous display of the thermal turbulent structure of the atmosphere, the vertical velocity and its standard deviation, and the wind speed and direction. It features three different 1.5-m diameter antennae/channels: one is oriented vertically, and the other two are oriented north-south and east-west and are tilted at 20 degrees from the zenith. The system radiates three short tone bursts, one for each antenna, at the three different frequencies (1750, 2000, and 2250 Hz) with a temporal resolution of 6 sec. This pattern results in an operative range of approximately 10^3 m, starting from a first useful range gate of approximately 25 m. The vertical resolution is 7 m for the echoed signal, and the horizontal resolution is 28 m. An extensive description of the instrument, including the electronic and data processing system, is given by Mastrantonio et al. (1994) and references therein.

Because the emitted acoustic waves are scattered by small-scale temperature fluctuations, i.e., the thermal turbulence, the mixing height can be estimated from sodar measurements using objective or subjective methods applied to the digitized range-corrected vertical profiles of signal intensity (range corrected signal). In the present study, a very reliable technique originally proposed by Beyrich (1993) and Beyrich and Weill (1993) has been used. Under convective conditions, the mixing height is defined as the height of an elevated secondary maximum that corresponds with the zone of strong turbulence at the capping inversion. Under stable conditions, the mixing height is determined from the minimum of the first derivative or from the maximum curvature of the range corrected signal, depending on the stage of the ABL evolution and on the shape of the range-corrected signal profile (Beyrich 1997, Casasanta et al. 2014).

2.1.4 Lidar

The lidar instrument deployed for this experiment was a custom-made, fully automated monostatic elastic backscatter lidar device, specially designed to observe the atmospheric aerosol vertical profile in the ABL through the entire troposphere. The radiation source is a Handy HYL 102 (Quanta System S.p.A.) Q-switched Nd:YAG laser with a second harmonic at 532 nm and a repetition rate of 20 Hz. The backscattered radiation is collected by a 100-mm Cassegrain telescope and by a 50-mm large field-of-view refractor telescope to observe the strong echo from the lowest atmosphere. In both the collectors, narrow-band interference filters are used to filter the collimated signals. This feature reduces the sky light, making it possible to obtain measurements in full daylight. The incoming radiation is detected by photomultipliers. The signals from both telescopes are matched in the overlapping altitude ranges to produce a continuous profile between approximately 100 m and 10 km, with a vertical resolution of 7.5 m. The instrument can also measure the linear depolarization ratio, but because such measurements have not been used in this work, the relevant data will not be described here. The acquisition system has been set to perform an integration of the backscattered signals over 15 s, corresponding to 300 laser shots, but all of the following analyses were performed on profiles averaged over 5 min.

The custom-made software controls the system handling, the quality assurance, and the time scheduling. For the whole measurement campaign, the lidar was programmed to perform measurements for 5 min before and after every hour, thereby creating two vertical profiles around each hour. The hourly mixing height was then retrieved by applying the well-known wavelet covariance transform method to these two profiles (Cohn and Angevine 2000, Davis et al. 2000, Brooks 2003, Pal et al. 2010) and taking the average value.

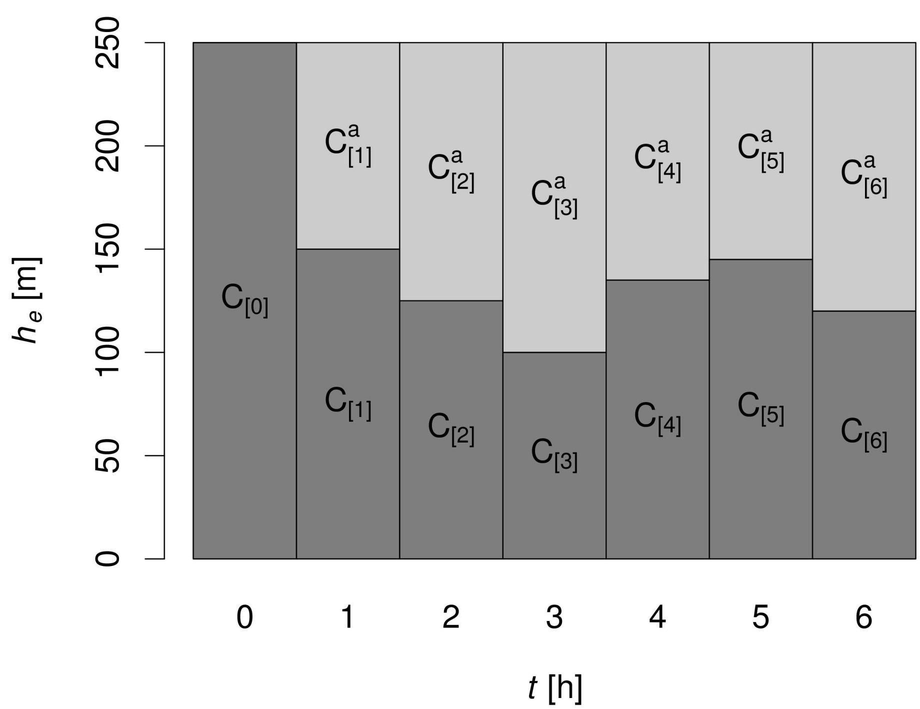

Fig 2 Temporal evolution of the nocturnal stable layer (dark grey box). The light grey area above represents the residual layer.

2.2 Mixing-height modelling

The evolution of the preferred box model should clearly include the introduction of the radon decay contribution and the description of a multi-layer structure. The contribution of the residual layer was introduced by Sesana et al (2003) and Pasini (2009), who approached the problem from a theoretical point of view. Griffith et al. (2013) defined a formulation of the so-called "dilution" term based on the formation of the residual layer every time the mixing height is lowered. Pasini et al. (2014) proposed a different approach based on a permanent residual layer that develops after the first compression of the day. This difference is coupled to the discrimination between compression an expansion based on the activity derivative instead of the height differential. We believe that these differences and the soil flux modelling are the most important innovation introduced herein. We preferred this approach because the removal of the residual layer is not a high-frequency process, so that our hypothesis consists in considering the residual term persisting over at least one night.

In Fig. 2, we define compression conditions when the stable layer depth decreases (i = 1, 2, 3, 6) and expansion situations when h_e increases (i = 4, 5). In the following discussion, λ is the ^{222}Rn decay constant (s^{-1}), t is our sampling interval (s), and C^a is the calculated concentration in the residual layer (Bq m^{-3}). Additionally, we adopt the symbolic form $h_{e[n,m]} = h_{e[n]} - h_{e[m]}$ for the difference between equivalent mixing heights at times n and m, respectively.

In compression cases, the generalization of Eq. 1 reads:

$$h_{e[i]} = \frac{\phi}{\lambda} \frac{1 - e^{-\lambda \Delta t}}{C_{[i]} - C_{[i-1]} e^{-\lambda \Delta t}}, \tag{2}$$

and the concentration in the residual layer after the i^{th} compression is,

$$C^a_{[i]} = \frac{C^a_{[i-1]} e^{-\lambda \Delta t} \Delta h_{e[0,i-1]} + C_{[i-1]} e^{-\lambda \Delta t} \Delta h_{e[i-1,i]}}{\Delta h_{e[0,i]}}. \tag{3}$$

If the stable layer depth increases and the overlying air is included in the box, i.e., in cases of expansion, the equivalent mixing height can be calculated as,

$$h_{e[i]} = \frac{\frac{\phi}{\lambda}(1 - e^{-\lambda \Delta t}) + h_{e[i-1]}(C_{[i-1]} - C^a_{[i-1]}) e^{-\lambda \Delta t}}{C_{[i]} - C^a_{[i-1]} e^{-\lambda \Delta t}}, \tag{4}$$

and the concentration above the top of the box (in the residual layer) is

$$C^a_{[i]} = C^a_{[i-1]} e^{-\lambda \Delta t}. \tag{5}$$

2.2.1 Soil radon-flux submodel

A second main aim of the present study is to test the introduction of a variable emanation rate instead of a constant radon flux. The Rn source term can be modelled or derived by intercomparison with other techniques (Griffith et al. 2013). However, the radon flux originating from the surface is a complex process influenced by many factors (Sun et al. 2004, Voltaggio et al. 2006, Zhuo et al. 2008), and although pedology and geology are disciplines that are not commonly involved in atmospheric modelling, the support provided by a multidisciplinary approach focused on radon emanations from the soil is important. The definition of the radon-emitting source can, in fact, improve atmospheric models (Szegvary et al. 2007).

The simplest way to predict the exhalation rate is the application of idealized models based on the porous media transport theory. This sub-model follows the direction of Zhuo et al. (2008), who proposed a combined model in which the soil radon emanation power and the soil water saturation are the main parameters that control the radon flux, viz.

$$\phi = R\rho_b\varepsilon(\frac{T_S}{273})^{0.75}\sqrt{\lambda D_0 p\ exp(-6Sp - 6S^{14p})}. \quad (6)$$

Here ϕ is the radon flux (Bq m^{-2}), R is the ^{226}Ra soil content (Bq kg^{-1}), ρ_b is the soil bulk density (kg m^{-3}), T_s is the soil temperature (K), D_0 is the ^{222}Rn diffusion coefficient in air, S is the soil water saturation, p is the soil total porosity and ε is the radon emanation power. This kind of model is based on a steady-state condition that considers the dominant contribution of diffusion and neglects the forced flow due to horizontal atmospheric pressure gradients. The altitude above the ground of the sampling site supported the assumption of steady-state soil exhalation. This approach can produce, of course, an underprediction of the soil exhalation rate especially in terms of high frequency variations and we focus our attention on this issue in later studies. Once the soil flux is parametrized by a sub-model based on Eq. 6 (the details of which are presented in Appendix 1), we are able to compare the results from standard and improved models (Fig. 3). The difference between the two models is defined as

$$\Delta h = \frac{\left(h_e^{variable} - h_e^{constant}\right)}{h_e^{constant}}. \quad (7)$$

Although small discrepancies (less than 5%) were frequently observed in correspondence with expansion conditions, slight but significant differences (approximately −10%) were detected during the nighttime.

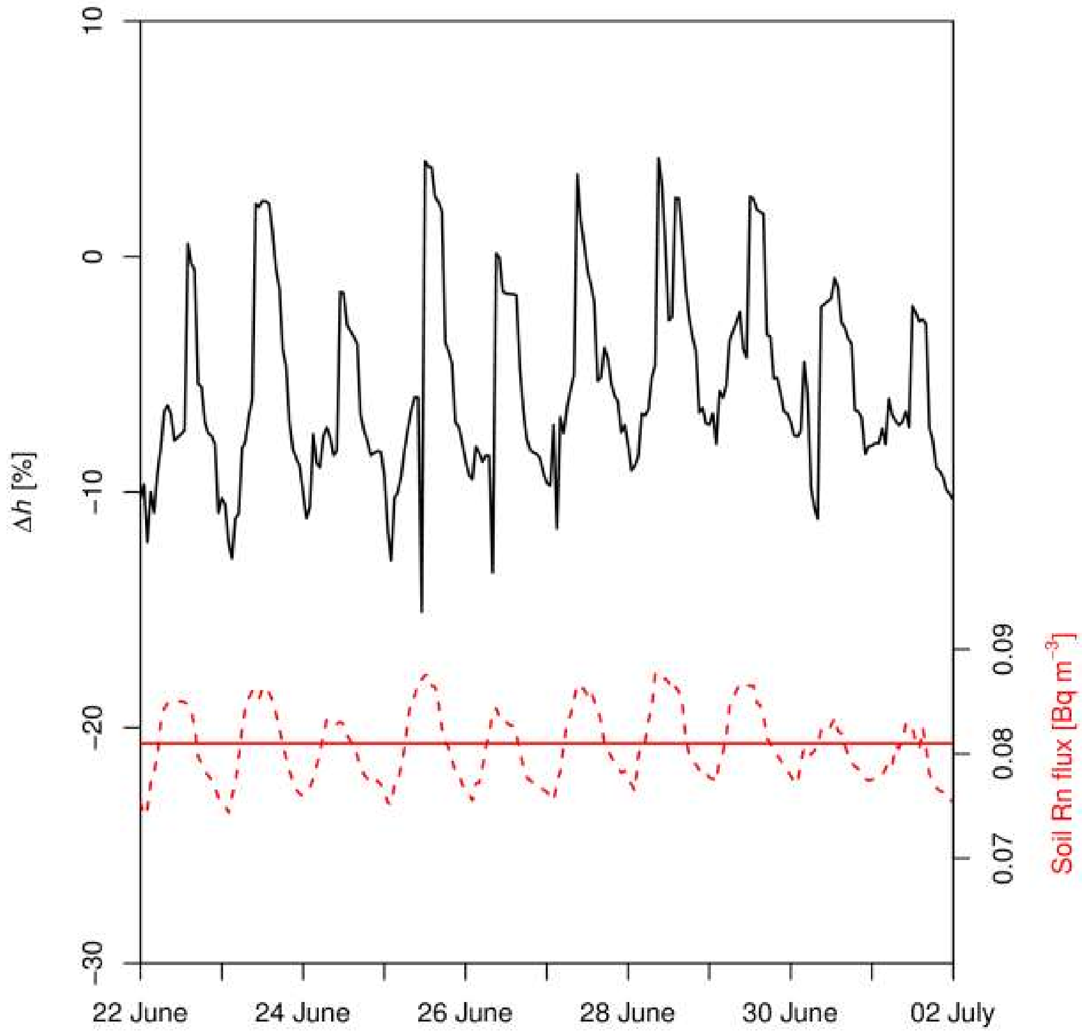

Fig 3 Percent difference in mixing height (black line) between equivalent mixing heights estimated using constant (continuous red line) and variable (dotted red line) soil radon fluxes.

The latter deviation is negligible if we consider the absolute amount of discrepancy (only 5-10 m, with a mixing height of approximately 50-100 m during the nighttime). These negative anomalies are often associated with major variations in soil humidity, and they may be consistent when strong advection occurs. Further validations are required to confirm the performance of the improved model. The accordance between the two considered models could be, in fact, influenced by the under-prediction in unsteady conditions and by the absence of sharp variations in terms of meteorological conditions (precipitation, humidity, etc.) during the survey.

2.2.3 Gross β counts versus air radon activity -- Theoretical solution

The critical step in using radon progeny as a tool for modelling the mixing height of the boundary layer is the conversion between gross β counts and air radon activity. This issue can be approached in two complementary ways. The first one is based on finding a theoretical solution considering the gross β counts emitted by filters where radon and thoron progeny are collected. Essentially, four nuclides contribute to the total β emissions because the β branching rate of ^{218}Po is negligible,

$$\beta_{tot} = \epsilon_s\{\epsilon_{1024}[^{214}Pb]_\beta + \epsilon_{3272}[^{214}Bi]_\beta + \epsilon_{2252}[^{212}Pb]_\beta + \epsilon_{4999}[^{212}Bi]_\beta\}, \quad (8)$$

where β_{tot} is the total counts, ϵ_s is the sampling efficiency, ϵ_{keV} is the detector efficiency at a specific energy, $[^{xxx}C]_\beta$ is the β activity of a specific nuclide. While the sampling efficiency, generally considered to be approximately 100% (Islam and Haque 1994) and homogeneous for all the considered nuclides, is a negligible term of the Eq. 8 ($\epsilon_s = 1$), the detector efficiency is a key parameter that rules the total β counts. The first two members of Eq. 8 are related to the ^{222}Rn decay series having half-lives of 26.8 and 19.9 min respectively. The remaining decay component are associated with the ^{220}Rn decay series with 10.2 and 1.0 h half-lives. The instrument presented in section 2.1.2 discriminates between the contributions of short-lived products (^{222}Rn progeny) and long-lived products (^{220}Rn progeny). Considering also the lower presence of thoron associated with the altitude of the sampling point, Eq. 8 can be limited to the first two members.

The decay of those isotopes during the sampling and the counting phases regulate the final measurement. The first phase can be described by the following,

$$\frac{\mathrm{d}[^{218}Po]_{filt}}{\mathrm{d}t_s} = \nu[^{218}Po]_{air} - \lambda_{^{218}Po}[^{218}Po]_{filt}, \quad (9a)$$

$$\frac{\mathrm{d}[^{214}Pb]_{filt}}{\mathrm{d}t_s} = \nu[^{214}Pb]_{air} + \lambda_{^{218}Po}[^{218}Po]_{filt} - \lambda_{^{214}Pb}[^{214}Pb]_{filt}, \quad (9b)$$

$$\frac{\mathrm{d}[^{214}Bi]_{filt}}{\mathrm{d}t_s} = \nu[^{214}Bi]_{air} + \lambda_{^{214}Pb}[^{214}Pb]_{filt} - \lambda_{^{214}Bi}[^{214}Bi]_{filt}, \quad (9c)$$

where the solutions estimate the β pre-counting activity of each nuclide, whereas other equations regulate the following counting phase,

$$\frac{\mathrm{d}[^{218}Po]_{\beta}}{\mathrm{d}t} = -\lambda_{^{218}Po}[^{218}Po]_{filt}, \tag{10a}$$

$$\frac{\mathrm{d}[^{214}Pb]_{\beta}}{\mathrm{d}t} = \lambda_{^{218}Po}[^{218}Po]_{filt} - \lambda_{^{214}Pb}[^{214}Pb]_{filt}, \tag{10b}$$

$$\frac{\mathrm{d}[^{214}Bi]_{\beta}}{\mathrm{d}t} = \lambda_{^{214}Pb}[^{214}Pb]_{filt} - \lambda_{^{214}Bi}[^{214}Bi]_{filt}. \tag{10c}$$

Considering the low β decay branch ratio of ^{218}Po, the solution can be simplified as demonstrated by Islam and Haque (1994),

$$\begin{aligned} \beta_{tot} = {} & \epsilon_{1024}\nu f_{^{214}Pb}[^{222}Rn]_{air}[4.28\times10^{5}(1-e^{-\lambda_{^{214}Pb}t_s})(e^{-\lambda_{^{214}Pb}t_c^i}-e^{-\lambda_{^{214}Pb}t_c^f})] + \\ & -\epsilon_{1024}\nu f_{^{214}Pb}[^{222}Rn]_{air}[1.81\times10^{5}(1-e^{-\lambda_{^{214}Bi}t_s})(e^{-\lambda_{^{214}Bi}t_c^i}-e^{-\lambda_{^{214}Bi}t_c^f})] + \\ & +\epsilon_{3272}\nu f_{^{214}Bi}[^{222}Rn]_{air}\left[4.84\times10^{4}\left(1-e^{-\lambda_{^{214}Bi}t_s}\right)\left(e^{-\lambda_{^{214}Bi}t_c^i}-e^{-\lambda_{^{214}Bi}t_c^f}\right)\right], \end{aligned} \tag{11}$$

where ν is the sampling rate (m^3 min^{-1}), t_s is the filter sampling time (min), t_c is the initial (i) and the final (f) counting time elapsed after the sampling period, $[^{222}Rn]_{air}$ is the radon air activity, $\epsilon_{(\mathrm{keV})}$ is the detector efficiency at a specific energy, $f_{^{214}Pb}$ is the equilibrium factor between ^{214}Pb and radon in the atmosphere, $f_{^{214}Bi}$ is the equilibrium factor between ^{214}Bi and radon in the atmosphere. The counting strategy of an instrument regulates the relationship between the conversion factor (c_f) and the remaining input variables,

$$\begin{aligned} \beta_{cpm} &= \frac{\epsilon_{1024}\nu f_{^{214}Pb}[^{222}Rn]_{air}[F_1 - F_2] + \epsilon_{3272}\nu f_{^{214}Bi}[^{222}Rn]_{air}F_3}{t_c^f - t_c^i} = \\ &= 60 c_f \nu t_s [^{222}Rn]_{air}, \end{aligned} \tag{12}$$

where $F_1 = 4.28\times10^{5}(1-e^{-\lambda_{^{214}Pb}t_s})(e^{-\lambda_{^{214}Pb}t_c^i}-e^{-\lambda_{^{214}Pb}t_c^f})$, $F_2 = 1.81\times10^{5}(1-e^{-\lambda_{^{214}Bi}t_s})(e^{-\lambda_{^{214}Bi}t_c^i}-e^{-\lambda_{^{214}Bi}t_c^f})$, $F_3 = 4.84\times10^{4}(1-e^{-\lambda_{^{214}Bi}t_s})(e^{-\lambda_{^{214}Bi}t_c^i}-e^{-\lambda_{^{214}Bi}t_c^f})$, which implies

$$c_f = \frac{\epsilon_{1024} f_{^{214}Pb}[F_1 - F_2] + \epsilon_{3272} f_{^{214}Bi}F_3}{60(t_c^f - t_c^i)t_s}. \tag{13}$$

This mathematical treatment allows us to reduce the number of input variables in the model to just the detector efficiency and the radon-progeny equilibrium factor, though these two variables cannot be easily estimated with a detector that measures the gross β activity. For this reason, Eq. 13 cannot be solved analytically. Nevertheless, this theoretical treatment represents a starting point for understanding the relationship between gross β counts and air radon activity. The definition of the equilibrium factor between radon and its progeny also cannot be determined with our instrumentation; therefore we assume here that the equilibrium is complete between radon progeny ($f_{^{214}Pb} \approx f_{^{214}Bi} \approx f$). This assumption is consistent with Jacobi and Andre (1963), who found, at 20 m above the ground, a negligible disequilibrium between the two considered nuclides under different mixing conditions. The conversion equation (Eq. 13) can be consequently simplified as

$$c_f \approx \bar{\epsilon} f \nabla, \tag{14}$$

where $\bar{\epsilon}$ is the overall detector efficiency term, ∇ is a term depending on the counting scheme of the instrument and f is the degree of disequilibrium between radon and its progeny. While the first two terms are specific to the used instrument, the latter can vary between 0.8 and 0.95 during the day depending on the mixing state of the atmosphere and the altitude (Vinod Kumar et al. 1999). We were not able to exactly determine these parameters during the survey, so we preferred to use experimental sodar observations and fix a constant conversion factor.

3 Results

The comparison between the selected techniques provided the opportunity to optimize the model in terms of input variables and time synchronization. The optimization was first conducted considering only the sodar observations during the night when the near-stable conditions are predominant. The lidar observations were later used to validate the model output and to estimate the model performance under turbulent conditions.

3.1 Time synchronization

The first issue addressed was the time synchronization between radon progeny dynamics and the sodar estimates of the mixing height. Assuming that the sodar observations are based on the turbulent thermal structure of the lower troposphere, the diffusion of radon progeny through the mixing layer is assumed to produce a delay.

Considering the definition of the mixing height offered by Seibert et al. (2000), "The mixing height is the height of the layer adjacent to the ground over which pollutants or any constituents emitted within this layer or entrained into it become vertically dispersed by convection or mechanical turbulence within a time scale of about an hour", we first checked whether our observations were consistent with this constraint.

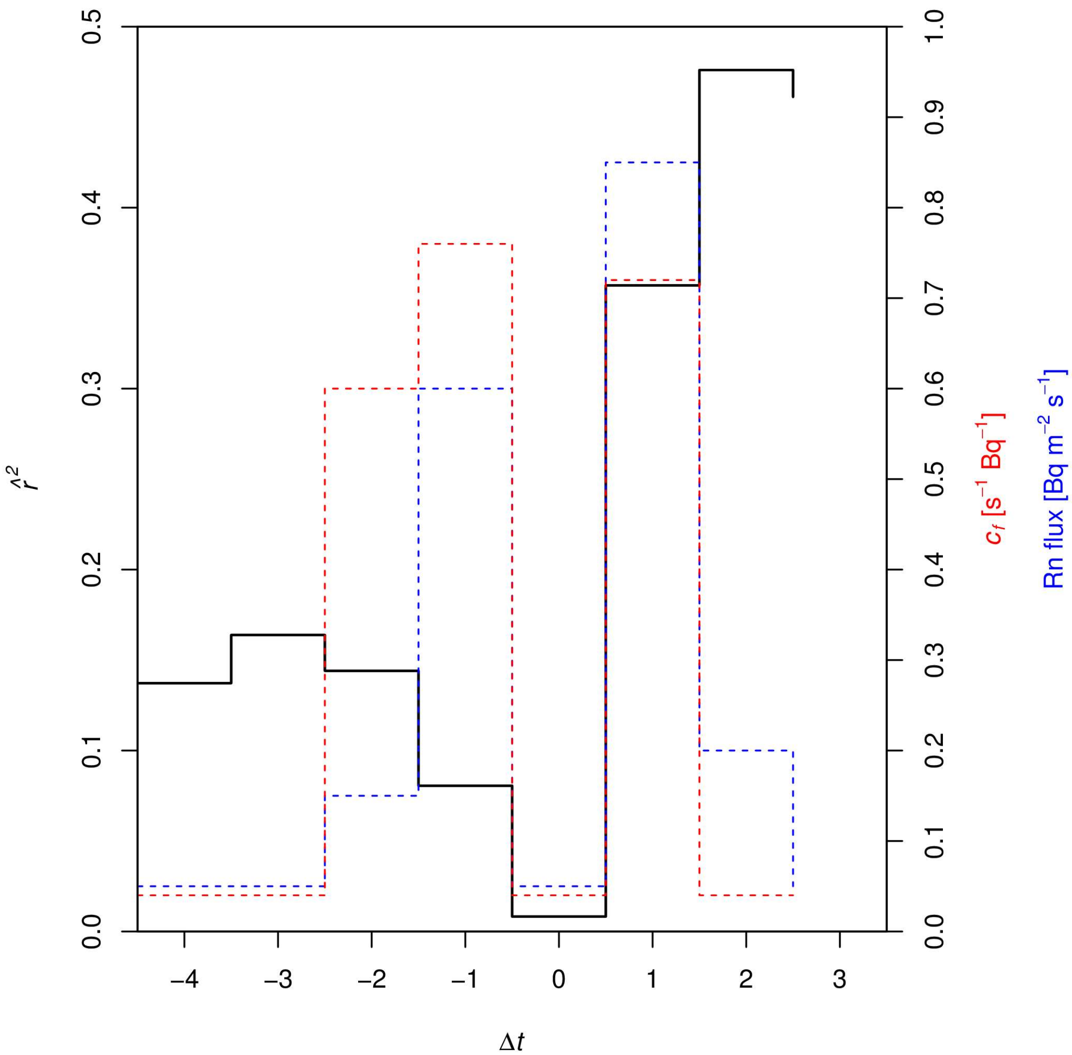

Fig 4 Statistical estimation of radon diffusion delay. The continuous black line shows the maximum calculated linear regression coefficient ($\hat{r}^2$) obtained for sodar observations and radon-derived estimates. The dotted lines show the input values required to obtain the best correlation. The variables are the radon exhalation rate (blue) and the conversion factor c_f from gross β counts to air radon content (red). The number of hours between radon observations and sodar measurements is described by Δt.

The analysis was performed by looking for the best fit in both types of estimates under nocturnal conditions (Fig. 4), while the statistical relationship was calculated considering a narrow time window from 2300 to 0400 UTC. The model simulations used 400 combinations of values for the soil radon flux and conversion factor, with a selected dataset of 66 observations. The former parameter varied between 0.01 and 0.8 Bq m^{-2} s^{-1}, and the latter ranged between 0.01 and 0.8. The radon flux interval was selected based on values available in the literature (Tuccimei and Soligo 2008), and the conversion factor maximum was determined based on an average detector efficiency of 50-60%. The best fit was obtained using a 2-h shift between radon-derived mixing height and sodar estimates. One hour can be ascribed to the start/finish of the sampling phase (1-h long), and the residual one hour suggests that the diffusion of radon in the atmospheric layer under nocturnal weak stable conditions is consistent with the mixing-height definition.

3.2 Gross β counts versus air radon activity -- Experimental solution

Model runs with different input variables defined the conversion factor between gross β counts and Rn air activity (required by the model). The conversion factor is controlled by an instrumental component, which is dependent on the detector efficiency, and by the soil exhalation rate of radon. The best combination of both variables was selected to achieve the best linear regression coefficient (r^2), the lowest root-mean-square error (*RMSE*) and the closest regression coefficient to 1. In this case, the statistical relationships was calculated considering the whole sodar dataset between 15 and 8. We selected 126 observations, and the model ran using 400 combinations of values for soil radon flux and conversion factor. In this phase, the soil radon flux also varied between 0.01 and 0.8 Bq m^{-2} s^{-1}, and the conversion factor ranged between 0.01 and 0.8. An inverse relationship between the two variables was observed (Fig. 5). A sharp decrease in the regression coefficient occurred along a hyperbolic-shaped limit that corresponded to an increase in the *RMSE*. The combinations of input variables that produced a slope between the sodar observations and the radon-derived estimates closer to 1 corresponded to the lowest *RMSE* values. Furthermore, the optimal combination of the parameters was found when the mean soil radon flux is 0.08 Bq m^{-2} s^{-1}) and the conversion factor (c_f) is 0.77.

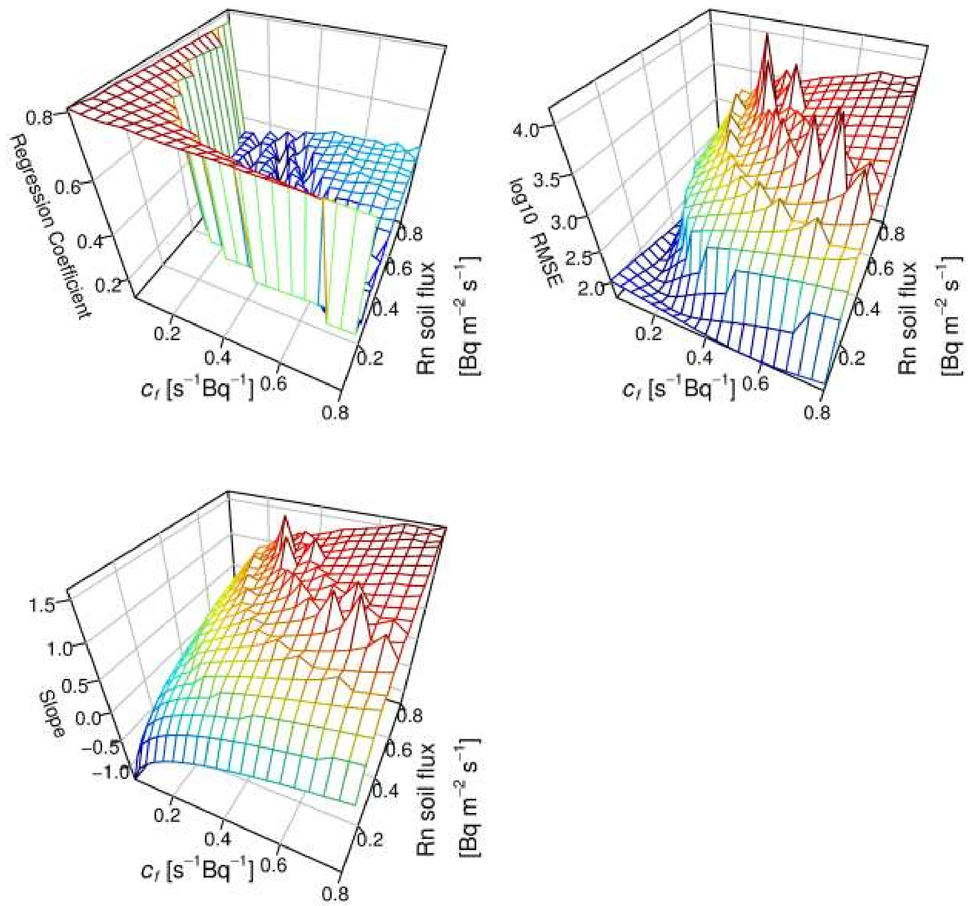

Fig 5 Statistical output of the performed model runs with different combinations of input parameters. Estimation of the linear regression coefficient *(r^2)* (a), of the root-mean-square error (*RMSE*) (b), and of the slope (c), between the sodar observations and the radon-derived mixing height.

3.3 Model validation

The performance of our model was validated using different independent techniques, such as sodar and lidar. While sodar estimates of mixing height are more reliable under nocturnal conditions, lidar observations are more consistent during the day. We defined a "stability limit" in terms of equivalent radon activity where the agreement between sodar and radon-derived estimates is consistent. On the other hand, we fixed a "turbulent limit" where advection is a major component and box-modelling assumptions are not respected. Finally, we discriminated different transition phases considering the time gradient of equivalent radon activity.

3.3.1 Meteorological framework

The meteorological conditions during the survey can be summarized in Fig. 6. The major meteorological parameters were reported in combination to the equivalent radon activity. We observed only one precipitation event during July 5 with about 1 mm of rain in the early morning.

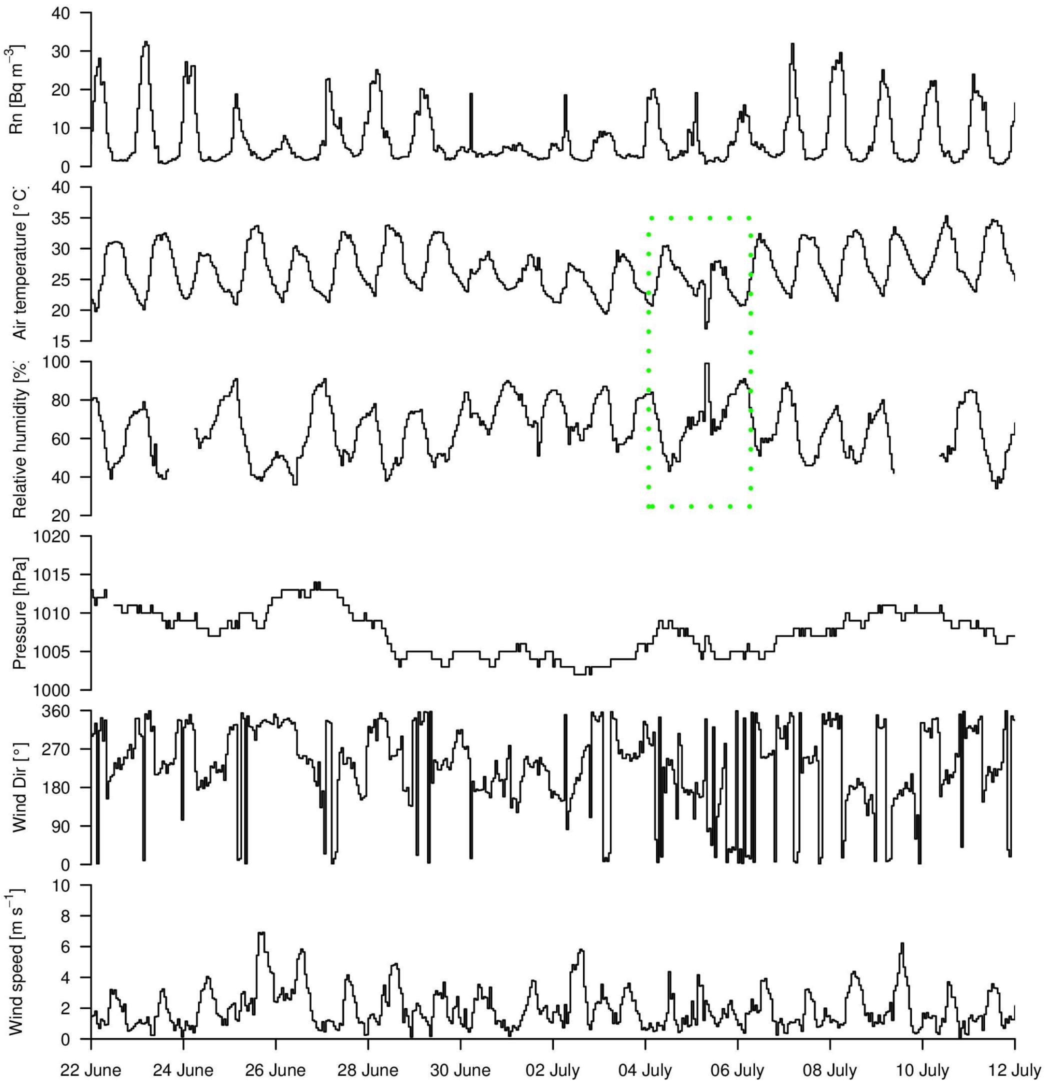

Fig 6 Summary plot of the major meteorological parameters. The dotted green rectangle highlighted the precipitation event occurred during the survey. Wind parameters are derived from sodar observations at an altitude of 48 m above the ground.

The most important feature was the airflow that showed the typical sea-breeze pattern for this area (Caballero and Lavagnini 2002). The flow was dominated by the sea breeze (from the south-western sector) from 1000 to 2100 UTC and was influenced mainly by topography (mainly from the northern sector) during the night and early morning. The sea-breeze component was active during the day and the front cross the city on late afternoon. It is possible that during the evening (after 1700 UTC) the sea breeze was coupled to the up-slope flows directed to the geomorphological elements (the Sabina mountains and Tiber valley) located north eastern respect to the investigated site. While the switch from land to sea winds occurred at 0900-1000 UTC, the transition sea-to-land occurred at 1700-2100 UTC.

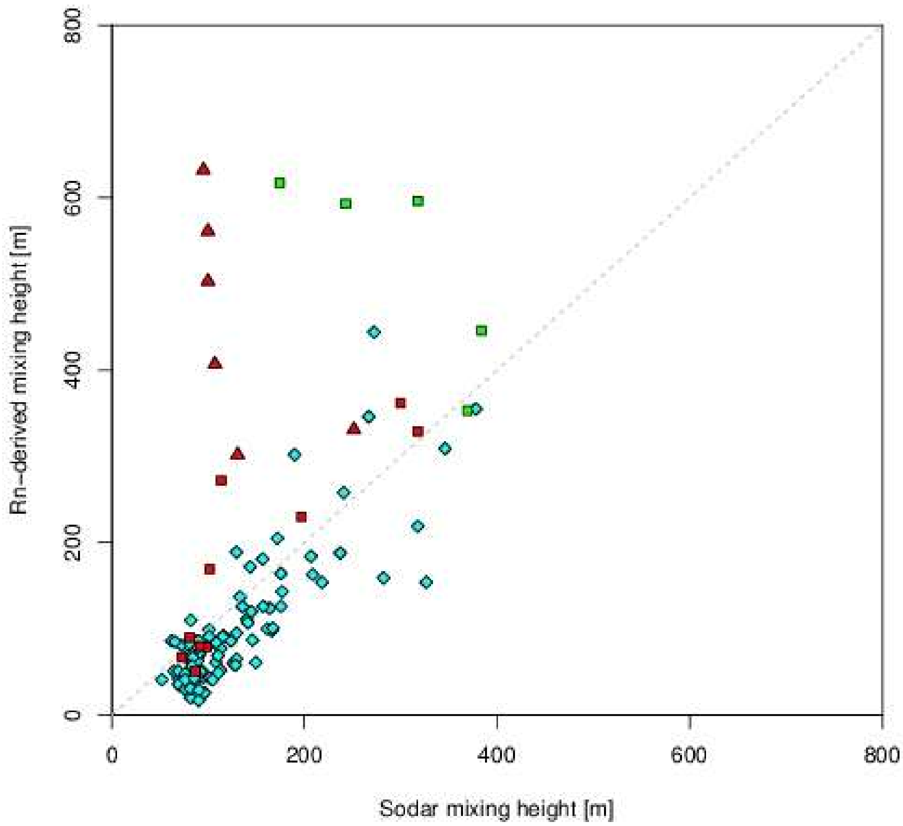

Fig 7 Comparison between the sodar observations and the radon-derived mixing heights. Observations are classified as near-stable (cyan diamond), heavy expansion (green square), soft compression (red triangle) and heavy compression (red square).

3.3.2 Near-stable conditions (radon vs. sodar)

The estimated values defined in Section 3.2 were used for the entire investigated period as input parameters, and the comparison between all of the available observations yielded a good agreement (Fig. 7). Few measurements were outliers, and the outliers that did exist were related to situations out of the near-stable conditions required by our model. Based on a 21-day survey, sodar provided 125 1h-averaged observations over 504 h that can be considered optimal for mixing height estimation, and only 17 observations (≈ 14%) appeared to be outliers (Table 1). In detail, 92 observations (≈ 73% of the total) were characterized by radon values greater than 9 Bq m^{-3} in the air, and no outliers were detected. The slope between the two independent estimates is 0.82, and the linear regression coefficient was approximately 0.88. Consequently, above this limit (now defined as "stability limit"), we had stability conditions or transition phases (compressions or expansions) consistent with the box model definition. The radon-derived mixing heights under the stability limit were all below 400 m, with an average deviation from sodar estimates of approximately −28 m. The negative deviation of radon-derived mixing heights with respect to the sodar values indicated an underestimation that could reflect the different nature of the mixing height associated with the considered techniques or some limitations to our model associated to disequilibrium variations (not considered by the average estimation of the conversion factor).

Condition	Radon		Sodar		Lidar	
	Activity	Gradient	Obs.	Δ	Obs.	Δ
	Bq m^{-3}	Bq m^{-3}		m		m
Near-stable	≥ 9		92	-28	123	-120
Soft compression	3 - 9	≤ +0.7	6	+310	24	+110
Heavy compression		> +0.7	10	+26	35	-250
Soft expansion		≥ -0.8	0		18	+300
Heavy expansion		< -0.8	6	+400	47	+610
Turbulent	≤ 3		11	+1400	155	+2000

Table 1 Summary of the observed conditions with the different techniques. Δ represents the deviation of radon-derived mixing height from sodar or lidar estimates.

In opposition to this accordance between the two approaches, we observed a net deviation in case of air radon activities below 3 Bq m^{-3}. Below this limit, which we define as the “turbulent limit”, we observed 11 events (≈ 10% of the total) with an important overestimation of approximately 1,400 m above sodar mixing-height values (≈ 300 m). Furthermore, intermediate situations can be defined if we consider the air radon activities included between the above-mentioned limits. If positive increases in air radon activity (> 0.7 Bq m^{-3}) occur, we can identify “heavy compression” situations suitable for box modelling. We defined 10 events of this type, with an average deviation from sodar estimates of approximately +26 m and a linear regression coefficient of 0.65. These events occurred generally on evening, just before the near-stable situations, indicating the switch between sea to land breeze. We can infer a weak underestimation of the box model associated with sharp variations in terms of radon activities and disequilibrium between radon and its progeny. The other intermediate conditions (“soft compression”, “soft expansion” and “heavy expansion”) were characterized by sodar mixing-height values of approximately 130 m, 370 m and 290 m, respectively, with an average deviation of +400 m from the sodar estimates. Situations of heavy expansion (with air radon activity between 3 and 9 Bq m^{-3} and decreases greater than −0.8 Bq m^{-3}) occurred six times (five days) and they occurred generally in the morning (0700-1000 UTC). These events were detected at the transition between the near-stable and the turbulent situations, indicating the land-to-sea air masses switch. The box model overestimation can be related to significant variations in terms of sources. The radon flux under this situations is strongly overestimated because sea water has a lower radon exhalation rate compared to rocks. The number of soft-compression situations (with air radon activity between 3 and 9 Bq m^{-3} and increases of less than +0.7 Bq m^{-3}) and soft-expansion events (with air radon activity between 3 and 9 Bq m^{-3} and decreases of less than +0.7 Bq m^{-3}) combined to sodar observations were limited. The possible interpretation of such conditions will be discussed in the comparison with lidar observations. The above-described definition of the box model constraints requires a larger dataset to rigorously define the model’s applicability limits, and should be tested for a longer period and applied in different geological condition. The presented limits refer to a situation where local outcropping rocks have a natural content of ^{226}Ra of approximately 100 Bq kg^{-1}. Therefore, lower contents will consequently be associated with lower reference values.

3.3.3 Turbulent conditions (radon vs. lidar)

Using the considered parameters, the evolution of the mixing height during the period showed good agreement between sodar mixing-heights and the radon-modelled estimates. The comparison between radon estimates and lidar mixing-heights (Fig. 8) exhibits a different behaviour.

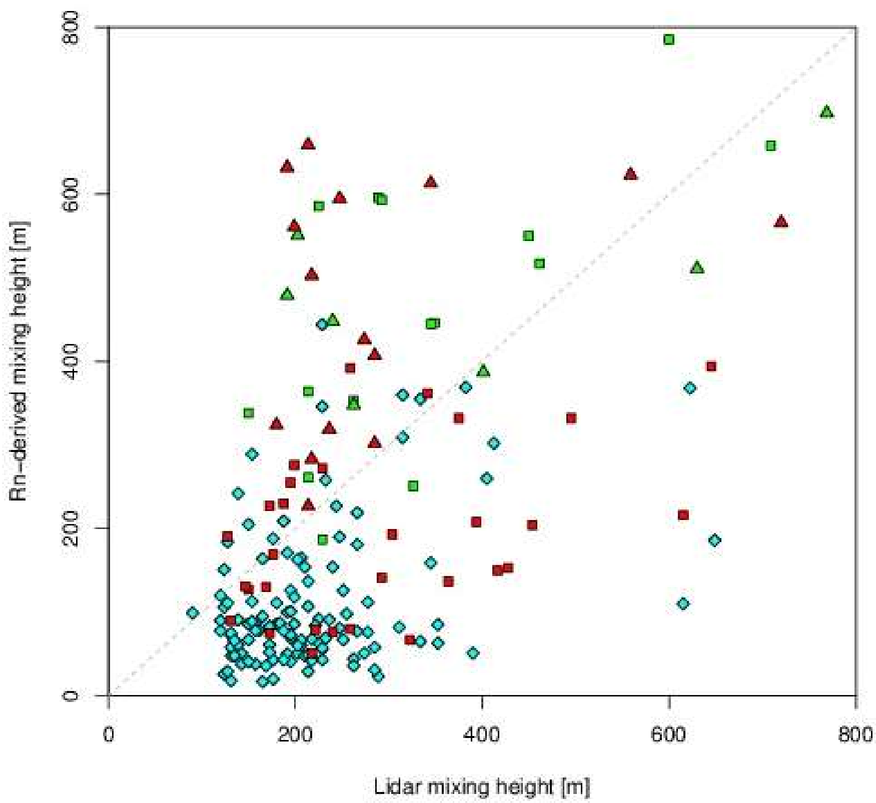

Fig 8 Radon vs. lidar observations. Observations are classified as near-stable (cyan diamond), heavy expansion (green square), soft expansion (green triangle), soft compression (red triangle) and heavy compression (red square).

Lidar performed during the survey produced 402 1-h averaged observations, and considering the stability limit, 123 observations (≈ 30% of the total) were characterized by stable conditions consistent with the box model definition (Table 1). The radon-derived mixing heights above the stability limit were all below 400 m, with an average deviation from lidar estimates of approximately −120 m. The radon-derived mixing heights in this case were also underestimated, and the lowest level of detection for lidar was approximately 100 m.

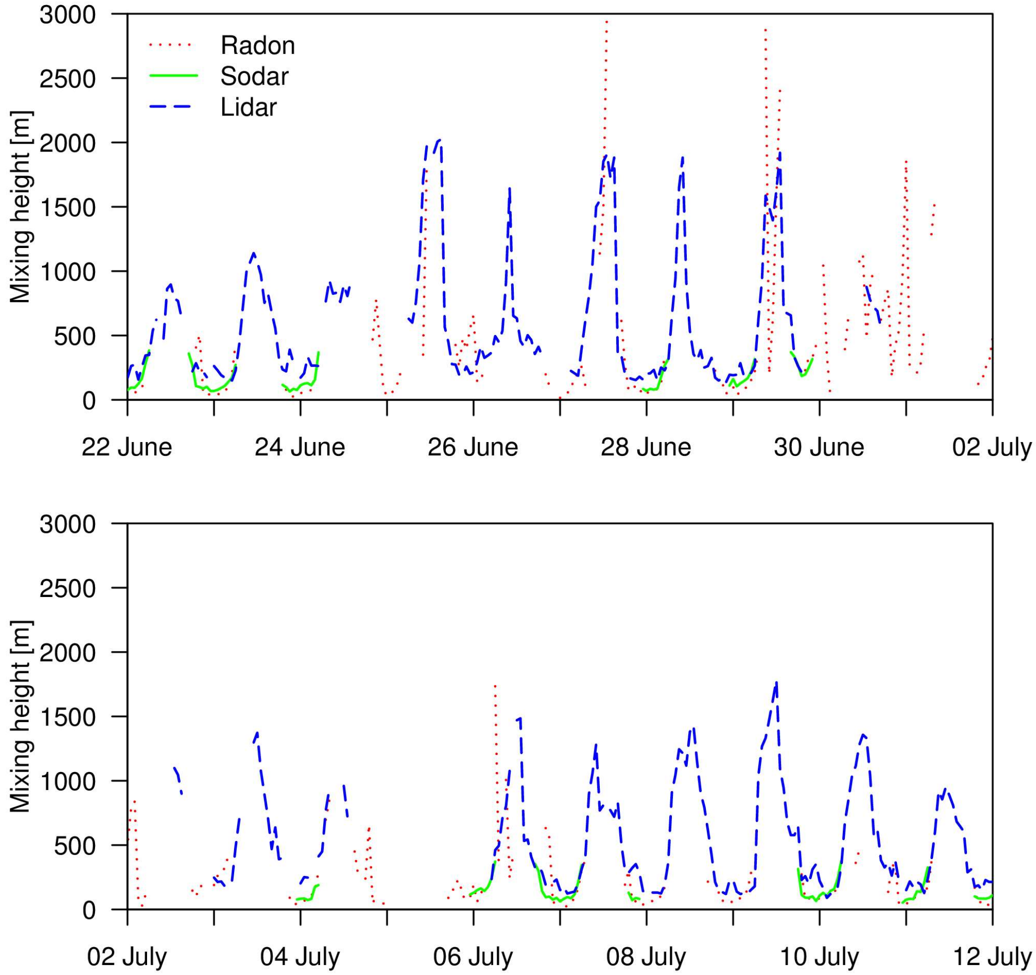

Fig 9 Temporal evolution of the mixing height estimated by sodar, lidar and radon progeny techniques. Radon mixing heights are limited to conditions above the "turbulent limit".

A total of 155 observations occurred under turbulent conditions (≈ 38% of the total), and the overestimation in this case was greater than 2 km over the mean lidar values (approximately 800 m). All the turbulent limit events were observed between 1000 and 2000 UTC and winds were a combination of sea breeze (from the south-west sector) and other terrestrial directions (north-north-west sector and south-south-east sector). An overestimation under these conditions was expected, since advection is a dominant component and box modelling is not appropriate.

The important information that can be derived, in this case, is the start time and the duration of the turbulent period. Intermediate situations suitable for box modelling were detected in 35 heavy compression events, with an average deviation from lidar estimates of approximately –250 m. The interpretation presented above is confirmed by the underestimation of the mixing height. Under these conditions, the performance of sodar was superior to lidar, and in this case radon modelling can support lidar in order to improve its results. The other intermediate conditions ("soft compression", "soft expansion" and "heavy expansion") were obtained with lidar mixing heights ranging from 600 to 900 m and with an average deviation of 200 m from lidar estimates. While this is consistent with the interpretation of heavy expansion events discussed above (Section 3.3.2), more indications can be obtained for soft compression and soft expansion. Some of these events (≈ 30%) were characterized by wind speeds > 2 m s^{-1} occurring between 1000 - 1500 UTC, indicating variations in terms of air masses when the sea-breeze regime is not completely dominant. The remaining situations occurred in the late evening probably when the sea-breeze component was decaying. The variations of the radioactive features (radon activity and progeny disequilibrium), in these cases, were significant and our model failed to include these fluctuations.

Considering only the near-stable and weak-convection conditions (below 600 m), the comparison between the lidar and radon-derived mixing heights highlights the good performance of the radon-based estimates. Lidar yielded the best output during diurnal convection when the box model is out of the stated applicability range, in agreement with all of the available literature (Griffiths et al. 2013). The change in air mass fetch, under turbulent conditions, is dominant and box modelling is not appropriate. In this case, radon modelling can only outline the turbulent conditions and cannot make an exact prediction of the mixing height. Further implementations of the model are necessary to also include turbulent conditions.

A summary of these results is reported in Fig. 9, where the agreement between the sodar estimates and the radon-derived mixing height is consistent, especially under nocturnal near-stable conditions. The lidar observations are confirmed to be consistent, especially during daily conditions, but the extension of the operating conditions of our improved box model enhances the capacity to integrate both techniques.

4 Conclusions

The estimation of the radon-derived mixing height can be improved by including the vertical entrainment of residual layers and variability in the soil radon exhalation rate in a box model. Our objective was to provide an improved box model and its validation; the efficiency in interpreting pollutant dynamics with this type of modelling has already been accomplished previously (Perrino et al. 2001, Chambers et al. 2015). The conversion of radon progeny gross β counts into air radon activity is presented from both theoretical and experimental perspectives. This approach supported the definition of a conversion factor controlled by instrumental efficiency and counting scheme. The presence of complete equilibrium in the radon progeny is, at the moment, an important approximation assumed by our model. The comparison between radon-derived estimates, sodar mixing heights and lidar values supported the definition of the applicability range of this box model. It was possible to identify count limits that describe "near-stable" conditions, occurring especially in late afternoon, at night, and early morning periods, during which good agreement between radon-derived and sodar estimates was observed. Additional limits were identified for a "transition" range, occurring during early afternoon and late morning periods, during which different processes occur. However, only certain types of compressions can be included in the conditions where the box model hypothesis are satisfied. Specific limits and situations outside of the validity range of the box model for turbulent conditions can easily be identified. Further studies are of course necessary for the definition of more general limits between the different intervals, but the improved model provides an enhanced application range for a simple detection of mixing height. However, the contribution of our model can already help improve the description of diffusion processes involving air pollutants.

5 Acknowledgments

The data used herein are available by contacting the corresponding author (salzano@iia.cnr.it). The sodar and lidar activities were performed with the support offered by Anna Maria Iannarelli, Cecilia Tirelli and Claudia Di Biagio. The meteorological data required by the soil exhalation modelling were provided by Anna Maria Siani, Physics Dept., University of Rome "Sapienza". We are grateful to Scott D. Chambers, who contributed to improving and clarifying the manuscript.

6 Appendix 1

The Eq. 6 included the following values for Rome: 100 Bq kg^{-1} for the ^{226}Ra soil content (Voltaggio et al. 2006), 1.5 × 10^{3} kg m^{-3} for the soil bulk density (Voltaggio et al. 2006) and 0.45 for the soil total porosity (Voltaggio et al. 2006). λ and D_0 are constants with values of 2.1 × 10^{-6} s^{-1} and 1.1 × 10^{-5} m^{2} s^{-1}, respectively. Soil temperature, water saturation and emanation power are time dependent variables that are influenced by meteorological conditions. The latter can be estimated using Zhuo et al. 2008,

$$\varepsilon = \varepsilon_0[1 + a(1 - e^{-bS})]. \quad (15)$$

The emanation power at 25 °C (ε_0) and the two constants a and b are specific for silty soils, such as the those present in the Rome area.

Considering these equations, the estimation of hourly fluxes requires the solution of heat and hydraulic balances to predict variations in terms of soil temperature and water saturation. The definition of a box model with a single layer (1 m height), representing the superficial soil, represents a preliminary approach. At this stage, several constraints are necessary to ensure a simple solution, but further development of the model is required to improve the prediction. Assuming that water infiltrates only vertically (no run-off and horizontal fluxes) and that no temperature and water gradients are present in this layer, the hydraulic balance can be defined as follow,

$$S = \frac{V_{water}}{V_{pores}} = \frac{V_{water}}{p\,V_{soil}} = \frac{10^{-3}(P_h - ET_0)}{p\,V_{soil}}. \quad (16)$$

The soil water saturation is defined as the ratio between water volume and pore volume, and can be rewritten as a function of soil porosity and is consequently related to P_h (hourly precipitation in mm), ET_0 (hourly evapotranspiration in mm), V_{soil} (the considered soil volume in m^{3}) and p as soil porosity.

Moreover, the thermal balance can be expressed,

$$\Delta T = \frac{G}{C_v h}, \quad (17)$$

where ΔT is the soil temperature variation (K), G is the soil heat flux (J m^{-2}), C_v is the volumetric heat capacity in J m^{-3} K^{-1} and h is the layer thickness (m). In detail, the volumetric heat capacity can be computed as

$$C_v = c_{soil}\rho_b + c_w\rho_w S, \quad (18)$$

where c_{soil} is the average heat capacity of solid constituents in soil (J kg^{-1} K^{-1}), ρ_b is the soil bulk density (kg m^{-3}), ρ_w is the water density (kg m^{-3}), c_w is the water heat capacity and S is the soil water saturation.

The calculation of ET_0 and G was made following the approach of Allen et al (1998),

$$G = 0.1\, R_n\ (day), \tag{19a}$$

$$G = 0.5\, R_n\ (night). \tag{19b}$$

The soil heat flux (G) in this case is related to R_n, which is the net radiation (J m^{-2} h^{-1}),

$$ET_0 = \frac{0.408\Delta(R_n - G) + \gamma \frac{37}{T_a + 273.16} uVPD}{\Delta + \gamma(1 + 0.34u)}. \tag{20}$$

The Eq. 20 equation follows the Penman-Monteith method, where ET_0 is the hourly evapotranspiration (mm h^{-1}), u is the wind speed (m s^{-1}), R_n is the net radiation in J m^{-2} h^{-1}, γ is the psychrometric constant (kPa °C^{-1}), Δ is the slope of the saturation vapour pressure curve (kPa °C^{-1}), T_a is the air temperature (°C) and VPD is the vapour pressure deficit (kPa). The values of γ, VPD and Δ depend on air temperature, pressure and humidity, and they were calculated using functions described in Alexandris and Kerkides (2003). The net radiation was estimated using astronomical functions and cloud attenuation values obtained from cloudiness observations, following Kasten and Czeplak (1980).

6 References

Alexandris S, Kerkides P (2003) New empirical formula for hourly estimations of reference evapotranspiration. Agr Water Manage 60: 157–180

Allegrini I, Febo A, Pasini A, Schiarini S (1994) Monitoring of the nocturnal mixed layer by means of particulate radon progeny measurement. J Geophys Res 99(D9): 18765–18777

Allen RG, Pereira LS, Raes D, Smith M (1998) Crop evapotranspiration: guidelines for computing crop water requirements. In: Irrigation and Drainage Paper 56, UN-FAO, Rome, 300 pp

Beyrich F (1993) On the use of SODAR data to estimate mixing height. Appl Phys B 57(1): 27-35

Beyrich F (1997) Mixing height estimation from Sodar data—a critical discussion. Atmos Environ 31(23): 3941–3953

Beyrich F, Weill A (1993) Some aspects of determining the stable boundary layer depth from Sodar data. Boundary-Layer Meteorol 63(1): 97-116

Brooks I (2003) Finding Boundary Layer Top: Application of a Wavelet Covariance Transform to Lidar Backscatter Profiles. J Atmos Ocean Tech 20(8): 1092-1105

Caballero R, Lavagnini L (2002) A numerical investigation of the sea breeze and slope flows around Rome. Nuovo Cimento C 25(3): 287-304

Casasanta G, Pietroni I, Petenko I, Argentini S (2014) Observed and Modelled Convective Mixing-Layer Height at Dome C, Antarctica. Boundary-Layer Meteorol 151: 597-608

Chambers SD, Williams AG, Zahorowski W, Griffiths A, Crawford J (2011) Separating remote fetch and local mixing influences on vertical radon measurements in the lower atmosphere. Tellus B 63:843–859

Chambers SD, Zahorowski W, Williams AG, Crawford J, Griffiths AD (2013) Identifying tropospheric baseline air masses at Mauna Loa Observatory between 2004 and 2010 using Radon-222 and back trajectories. J Geophys Res Atmos 118: 992–1004

Chambers SD, Williams AG, Crawford J, Griffiths AD (2015) On the use of radon for quantifying the effects of atmospheric stability on urban emissions. Atmos Chem Phys 15: 1175–1190

Cohn S, Angevine W (2000) Boundary Layer Height and Entrainment Zone Thickness Measured by Lidars and Wind-Proling Radars. J Appl Meteorol 39: 1233-1247

Davis K, Gamage N, Hagelberg C, Kiemle C, Lenschow D, Sullivan P (2000) An Objective Method for Deriving Atmospheric Structure from Airborne Lidar Observations. J Atmos Ocean Tech 17(11): 1455-1468

Desideri D, Roselli C, Feduzi L, Meli MA (2006) Monitoring the atmospheric stability by using radon concentration measurements: A study in a Central Italy site. J Radioanal Nucl Ch 270(3): 523–530

Desideri D, Roselli C, Meli MA, Feduzi L (2007) Comparison between the diurnal trends of ozone and radon gas concentrations measured at ground in the semi-rural site of Central Italy. J Radioanal Nucl Ch 273(2): 345–351

Duenas C, Perez M, Fernandez MC, Carretero J (1996) Radon concentrations in surface air and vertical atmospheric stability of the lower atmosphere. J Environ Radioactiv 31: 87–102

Griffith AD, Parkes SD, Chambers SD, McCabe MF, Williams AG (2013) Improved mixing height monitoring through a combination of Lidar and radon measurements. Atmos Meas Tech 6: 207–218

Guedalia D, Ntsila A, Druihlet A, Fontan J (1980) Monitoring of the atmospheric stability above an urban and suburban site using Sodar and radon measurements. J Appl Meteorol 19: 839–848

Islam GS, Haque AKF (1994) Measurement of mixed radon and thoron daughter concentrations using alpha and beta activities filtered from air. Radiat Meas 23(4): 737–742

Jacobi W, Andre K (1963) The vertical distribution of Radon 222, Radon 220 and their decay products in the atmosphere. J Geophys Res 68(13): 3799-3814

Kasten F, Czeplak G (1980) Solar and terrestrial radiation dependent on the amount and type of cloud. Sol Energy 24: 177-189

Keller CA, Huwald H, Vollmer MK, Wenger A, Hill M, Parlange MB, Reimannet S (2011) Fiber optic distributed temperature sensing for the determination of the nocturnal atmospheric boundary layer height. Atmos Meas Tech 4: 143–149

Lin JC (2012) Lagrangian Modeling of the Atmosphere: An Introduction. In: Lin JC et al. (eds) Lagrangian Modeling of the Atmosphere, AGU, Washington DC, pp 1-11

Lopez A, Guedalia D, Servant J, Fontan J (1974) Advantages of the use of radioactive tracers 222Rn and 212Pb for the study of Aitken nuclei within the low troposphere. J Geophys Res 79:1243–1252

Mastrantonio G, Viola AP, Argentini S, Fiocco G, Giannini L, Rossini L, Abbate G, Ocone R, Casonato M (1994) Observations of sea breeze events in Rome and the surrounding area by a network of Doppler Sodars. Boundary-Layer Meteorol 71: 67-80

Nath S, Patil RS (2006) Prediction of air pollution concentration using an in situ real time mixing height model. Atmos Environ 40: 3816–3822

Pal S, Behrendt A, Wulfmeyer V (2010) Elastic-backscatter-Lidar-based characterization of the convective boundary layer and investigation of related statistics. Ann Geophys 28: 825-847

Pasini A (2009) Neural networks for characterization and forecasting in the boundary layer via radon data. In: Haupt SE et al. (eds) Artificial Intelligence Methods in the Environmental Sciences, Springer, Dordrecht, pp 255–268

Pasini A, Ameli F (2003) Radon short range forecasting through time series preprocessing and neural network modeling. Geophys Res Lett 30(7): 1386

Pasini A, Perrino C, Zujić A (2003) Non-linear atmospheric stability indices by neural network modelling. Nuovo Cimento C 26(6): 633-638

Pasini A, Salzano R, Attanasio A (2014) Modeling radon behavior for characterizing and forecasting geophysical variables at the atmosphere–soil interface. In: Sengupta D (eds) Recent trends in modelling of environmental contaminants, Springer, New Delhi, pp 213-237

Perrino C, Febo A, Allegrini I (2000) A new beta gauge monitor for the measurement of PM10 air concentration. In: Hanssen JE et al. (eds) EMEP-WMO Workshop on fine particles – emissions, modelling and measurements, EMEP/CCC-Report 9/2000, NILU, Kjeller, pp 147-152

Perrino C, Pietrodangelo A, Febo A (2001) An atmospheric stability index based on radon progeny measurements for the evaluation of primary urban pollution. Atmos Environ 35(31): 5235-5244

Perrino C, Catrambone M, Pietrodangelo A (2008) Influence of atmospheric stability on the mass concentration and chemical composition of atmospheric particles: a case study in Rome, Italy. Environ Int 34: 621–628

Porstendorfer J (1994) Properties and behaviour of radon and thoron and their decay products in the air. J Aerosol Sci 25(2): 219-263

Seibert P, Beyrich F, Gryning SE, Joffre S, Rasmussen A, Tercieret P (2000) Review and intercomparison of operational methods for the determination of the mixing height. Atmos Environ 34: 1001-1027

Sesana L, Caprioli E, Marcazzan GM (2003) Long period study of outdoor radon concentration in Milan and correlation between its temporal variations and dispersion properties of atmosphere. J Environ Radioactiv 65: 147–160

Sesana L, Ottobrini B, Polla G, Facchini U (2006) 222Rn as indicator of atmospheric turbulence: measurements at Lake Maggiore and on the pre-Alps. J Environ Radioactiv 86: 271–288

Frank G, Steinkopff T, Salvamoser J (2012) Low level measurement of 222 rn in the atmosphere in the frame of the global atmospheric watch programme. In: IAEA (eds) Sources and Measurements of Radon and Radon Progeny Applied to Climate and Air Quality Studies, IAEA, Wien: 105-114

Sun K, Guo Q, Zhuo W (2004) Feasibility for Mapping Radon Exhalation Rate from Soil in China. J Nucl Sci Technol 41(1): 86–90

Szegvary T, Leuenberger MC, Conen F (2007) Predicting terrestrial 222Rn flux using gamma dose rate as a proxy. Atmos Chem Phys 7: 2789–2795

Tuccimei P, Soligo M (2008) Correcting for CO2 interference in soil radon flux measurements. Radiat Meas 43: 102–105

Veleva B, Valkov N, Batchvarova E, Kolarova M (2010) Variation of short-lived beta radionuclide (radon progeny) concentrations and the mixing processes in the atmospheric boundary layer. J Environ Radioactiv 101: 538–543

Vinod Kumar A, Sitaraman V, Oza RB, Krishnamoorthy T (1999) Application of a numerical model for the planetary boundary layer to the vertical distribution of radon and its daughter products. Atmos Environ 33: 4717–4726

Voltaggio M, Masi U, Spadoni M, Zampetti G (2006) A methodology for assessing the maximum expected radon flux from soils in northern Latium (central Italy). Environ Geochem Hlth 28: 541–551

Williams AG, Zahorowski W, Chambers SD, Griffith A, Hacker JM, Element A, Werczynski S (2011). The vertical distribution of radon in clear and cloudy daytime terrestrial boundary layers. J Aerosol Sci 68: 155-174

Zhang X, Qi Y, Walling DE, He X, Wen A, Fu J (2006) A preliminary assessment of the potential for using 210Pbex measurement to estimate soil redistribution rates on cultivated slopes in the Sichuan Hilly Basin of China. Catena 68(1): 1-9

Zhuo W, Guo Q, Chen B, Cheng G (2008) Estimating the amount and distribution of radon flux density from the soil surface in China. J Environ Radioactiv 99: 1143-1148